


## Article

# Synthesis of ZIF-8 Coating on ZnO Nanorods for Enhanced Gas-Sensing Performance

Bo Huang <sup>1</sup>, Wen Zeng <sup>1,\*</sup>  and Yanqiong Li <sup>2</sup>

<sup>1</sup> College of Materials Science and Engineering, Chongqing University, Chongqing 400030, China; 20162974@cqu.edu.cn

<sup>2</sup> School of Electronic information & Electrical Engineering, Chongqing University of Arts and Sciences, Chongqing 400030, China; 20170031@cqwu.edu.cn

\* Correspondence: wenzeng@cqu.edu.cn

**Abstract:** Firstly, ZnO nanorods were prepared by a relatively simple method, and then self-sacrificed by a water bath heating method to generate a commonly used porous ZIF-8 and firmly attached to the ZnO surface. The successful synthesis of synthetic composites was demonstrated with various detection methods. The gas-sensing results show that the ZIF-8-coated ZnO with a core-shell structure exhibits better response than the raw ZnO because of the increased specific surface area and active sites.

**Keywords:** ZnO; metal-organic frameworks; composite; gas sensors



**Citation:** Huang, B.; Zeng, W.; Li, Y. Synthesis of ZIF-8 Coating on ZnO Nanorods for Enhanced Gas-Sensing Performance. *Chemosensors* **2022**, *10*, 297. <https://doi.org/10.3390/chemosensors10080297>

Academic Editors: Xiaoxing Zhang and Tae Geun Kim

Received: 29 June 2022

Accepted: 28 July 2022

Published: 30 July 2022

**Publisher's Note:** MDPI stays neutral with regard to jurisdictional claims in published maps and institutional affiliations.



**Copyright:** © 2022 by the authors. Licensee MDPI, Basel, Switzerland. This article is an open access article distributed under the terms and conditions of the Creative Commons Attribution (CC BY) license (<https://creativecommons.org/licenses/by/4.0/>).

## 1. Introduction

Humans live in the atmosphere and cannot survive without air. In addition to the main components in the air, there are many very small amounts of other gases, which may originate from volcanic eruptions, lightning, and the decomposition of biological corpses, but their content can be ignored, and the atmosphere itself has a certain ability to self-purify. However, the Earth has a limited capacity for self-cleaning. Moreover, with the progress and development of human science and technology, a large number of natural resources are consumed and a large amount of gases, including toxic gases and greenhouse gases, are produced in a short period of time [1,2]. Except for a small amount of naturally occurring gases, the vast majority of harmful gases are currently emitted from human activities; there are many ways to produce toxic and harmful gases, including industrial exhaust, automobile exhaust, and house renovation [3–6]. The Earth's self-cleaning capacity is also decreasing due to the decrease in wetlands and plants. If we expect the Earth to clean itself, we must wait for an extremely long time. Moreover, the cleanliness of the atmosphere directly affects the safety of human life, so countries advocate energy conservation and emission reduction, which is to curb pollution from the source. Meanwhile, the detection of various gases becomes very important in the production of life. Timely detection of these gases can not only avoid safety accidents, but also reduce air pollution.

Most conventional gas sensors use semiconducting metal oxides (SMO<sub>x</sub>), which are inexpensive and easy to fabricate [7–9]. Although there are some problems in detection performance, various methods have been explored to improve performance, and research on SMO<sub>x</sub> has never stopped [10–12]. Most of the traditional gas sensors use semiconductor metal oxides. As an iconic *n*-type semiconductor, ZnO is widely used because of its low cost, its ability to be prepared in a variety of shapes, and its ease of detection of a wide range of gases [13–17]. Although it has been shown through various studies that only using ZnO has various problems, various methods can address these challenges [18,19]. At present, the research of ZnO in gas sensing mainly focuses on improving the response and selectivity, lowering the optimal temperature, and improving the response-recovery speed. These can be improved by changing the morphology, light activation, doping precious

metals, compounding and so on [15,20–23]. The change of ZnO itself is mainly to improve the gas-sensing performance by changing the size and morphology of ZnO, which is mainly guided by the change of the synthesis method. At present, because of the small size and large specific surface area of 3D nanostructured ZnO, it can effectively improve the gas adsorption, so it is a research hotspot [24,25]. Light activation mainly uses ultraviolet light or visible light provided by the outside world instead of heat, thus lowering the working temperature of ZnO [15,26,27]. However, ultraviolet light has radiation and visible light has a low excitation rate, so further research is needed [25]. Precious metals can improve gas sensitivity by electrical or chemical effects, but this method has the disadvantage of high cost [28–30]. As a relatively common method, compounding has many advantages. First of all, there are many types of materials that can be combined with ZnO, such as other metal oxides, carbon materials, polymers and so on [25,31–33]. They can form various heterojunctions or homojunctions, which are favorable for the transition of electrons in the composite. Moreover, the advantages of the two materials can be combined together through synergistic action, so as to improve the disadvantages of the materials and obtain the desired properties.

Metal-organic frameworks (MOFs) are porous coordination polymers, which have been extensively studied in recent years and are used in various fields. Studies have shown that this material can enhance gas adsorption through metal ions and functional groups [34], and since these open metal ions can act as active sites to achieve electron transfer, it is believed that MOFs can react with specific gas molecules. MOFs also have potential for gas adsorption or detection. However, most MOFs are poorly conductive due to the insulating properties of organic ligands, so it is difficult to be intuitively represented by conversion into electrical signals, which is the reason why pure MOFs are less used in resistive gas-sensing applications [35–38]. Of course, there are some workarounds, such as using other kinds of gas sensors. In addition, the preparation of MOF-based composites is also a good application method [34]. There are many kinds of MOF materials. ZIF belongs to a relatively common category, which is an MOF material with a zeolite-like structure obtained by the reaction of Zn(II) or Co(II) with imidazole ligands [39,40]. ZIFs have many advantages, such as tunable structures and better thermal and chemical stability [34,41,42]. These advantages can provide potential utility for gas adsorption and sensing. As the most widely used ZIF material, the application of ZIF-8 in gas sensing has been reported [43–46]. ZIF-8 can improve gas-sensing performance by taking advantage of its advantages of moisture resistance, thermal stability, selective pore size, and large specific surface area [41,42,47,48]. Furthermore, ZIF-8, similar to most MOFs, is difficult to be directly used in resistance gas sensors because of its high resistance, so it can be compounded with other conductive materials to solve this problem [34]. Since ZnO is a semiconductor, it has certain conductivity [49]. Moreover, it can provide  $\text{Zn}^{2+}$  for ZIF-8, so it is a very suitable precursor of ZIF-8. There have been many reports on ZnO@ZIF materials, which mainly use the pore size of ZIF materials to screen small molecules and selectively detect them [45,50,51]. Besides the molecular sieve effect, the ZIF layer has been adjusted by changing the experimental conditions to observe its influence on gas-sensing performance [45,52]. Different thicknesses of ZIF layers not only affect the selectivity, but also affect the response-recovery speed [53]. Furthermore, the partial loading and shell-like loading of ZIF also affect the performance. However, the commonly used ZIF-8 is a hydrophobic material to prevent the cross-effect of humidity on the target gas and prevent the partial loading of the material [53]. Therefore, the use of a complete and uniform shell is more stable. As far as the use of materials is concerned, ZIF with other pore sizes can also be prepared by changing the active material into other semiconductor metal oxides and organic ligands [54–57].

At present, the green preparation of this kind of material is in excavation. The use of organic reagents generally contains dimethylformamide (DMF), and the preparation temperature is generally carried out at 70 °C or above. We discovered a new preparation method which can not only change the kind of organic reagents and reduce the cost, but

also reduce the energy consumption of the experiment to a certain extent. Moreover, this experiment has another outstanding advantage, faster response recovery process. In this study, we first prepared ZnO using a simple hydrothermal method, and then sacrificed the surface ZnO to generate ZIF-8. We used SEM, TEM, EDS, XPS, and XRD for detection and demonstration, followed by gas-sensing experiments. The results show that ZnO as a precursor can be successfully transformed into porous ZIF-8 and covered on its own surface, enabling an improved response to gas molecules below a specific size by increasing the active site. However, our experiment needs to be further improved, because the optimum working temperature was not decreased, which is the goal of further exploration in the future.

## 2. Experimental

### 2.1. Preparation of ZIF-8-Coated ZnO

To synthesize the ZIF-8-coated ZnO structure, 1.587 g  $\text{Zn}(\text{NO}_3)_2 \cdot 6\text{H}_2\text{O}$  and 1.707 g NaOH were first dissolved and mixed in 35 mL deionized water with constant stirring. After mixing uniformly, the mixture was kept at 140 °C for 12 h. After cooling, it was washed with water and dried at 80 °C for 8 h. Then, partial dissolution of zinc oxide and the formation and growth of the ZIF-8 shell were carried out. A total of 0.32 g of the dry white powder (ZnO) was dissolved in 20 mL of ethanol as solution A, and 3.2 g of 2-methylimidazole in 40 mL of ethanol was used as solution B. The two solutions were then mixed, and each was stirred at 50 °C for 4 h. After cooling, washing and drying were performed at room temperature.

Since there is no XRD standard card for ZIF-8, we synthesized ZIF-8 for XRD detection. We placed  $\text{Zn}(\text{NO}_3)_2 \cdot 6\text{H}_2\text{O}$  and 2-methylimidazole with a molar ratio of 1:8 into the same volume of methanol, then stirred evenly and mixed, and then stirred at room temperature for 5 min. Then, the mixed solution was subjected to ultrasonic vibration for 30 min, and then magnetically stirred at room temperature for 5 h. After centrifugation, it was washed with methanol. Finally, the obtained white precipitate was dried at 60 °C for 24 h to obtain pure ZIF-8.

### 2.2. Preparation of Sensors and Gas-Sensing Measurements

The preparation process of these sensors is as follows: The obtained composite product and the original ZnO rod-shaped sample were respectively placed in two agate mortars, a few drops of absolute ethanol and deionized water were added, and then ground into a paste. Then the paste was spread evenly on the sensor substrate, in which the size of Ag-Pd electrodes was 13.4 mm × 7 mm. The working temperature of the sensor was controlled by alloy resistance wire, and the prepared substrate was heated at 200 °C for 24 h. In order to prevent possible errors in the test results, we prepared three sensors for each material to conduct parallel experiments and took their average value.

The gas-sensing performance measurement of the sensor was carried out on the Chemical Gas Sensor-1 Temperature Pressure (CGS-1TP) Intelligent Gas-Sensing Analysis System (Beijing Elite Technology Co., Ltd., Beijing, China), and the device has various control systems (including temperature, control of gas, measurement, and probe position), which are composed as shown in the Figure 1. The temperature control range of this analysis system is from 25 °C to 500 °C, and the accuracy can reach 1 °C in this range. According to the literature, ZIF-8 is hydrophobic, but for the sake of ensuring the consistency of experimental conditions throughout the whole experiment and prevent the interference of external factors, synthetic air was used here to control humidity. By mixing water-saturated air with dry air at room temperature, synthetic air with relative humidity of 25% was obtained. When in use, the substrate on which the sensing material is deposited needs to be preheated on the temperature-controlled platform for 30 min. The test chamber is closed but has air inlets and air outlets. To inject synthetic air, a micro syringe to inject 18 L of synthetic air from the air inlet through a rubber stopper are used. Two probes are pressed against the electrode positions of the substrate to transmit changes of electrical

signals. When the resistance is stable, the sensor is ready, and the resistance at this time is displayed as air resistance ( $R_a$ ). Then, the target gas is injected by using a micro injector, and then a part of the synthetic air is mixed with the target gas. When the sensor resistance stabilizes again, the resulting mixed resistance is  $R_g$ . Finally, the test chamber is re-injected with synthetic air until the sensor resistance changes back to  $R_a$ . The sensitivity value ( $S$ ) of the sensor can be obtained, which is defined here as  $R_a/R_g$ .

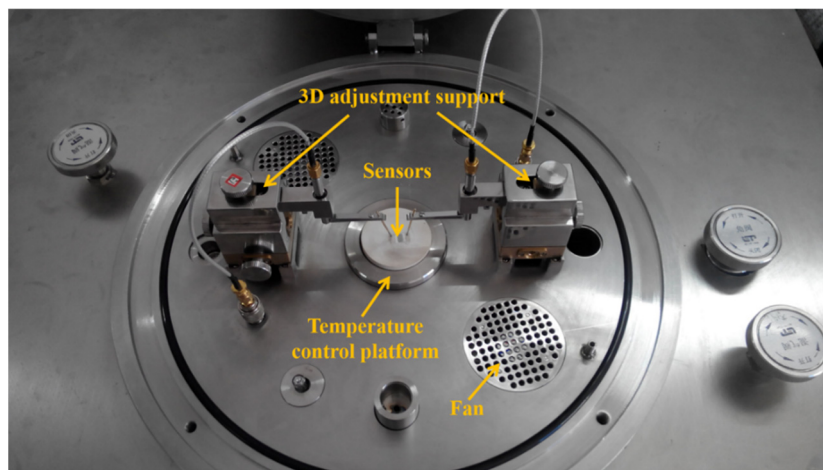


**Figure 1.** Gas-sensing analysis system.

### 2.3. Material Characterization

XRD data were collected using PANalytical X'Pert Powder to analyze the material composition, using Cu  $K\alpha$  radiation ( $\lambda = 1.5418 \text{ \AA}$ ). Microscopic morphology as well as elemental analysis were obtained using a Quattro S environmental scanning electron microscope (ESEM) and a Talos F200S transmission electron microscope (TEM, accelerating voltage 200 kV). The X-ray photoelectron spectrometer was used for the detection of XPS spectra, using the instrument model ESCALAB250Xi. The pore size distribution was mainly tested by a fully automatic multi-station specific surface and pore size analyzer (mesopore + micropore) model max-II (MicrotracBEL Japan, Inc., Yamaguchi, Japan), and ASFM free volume correction was used in the test process.

## 3. Results and Discussion

### 3.1. Microstructure Characterization

#### 3.1.1. XRD Analysis

Figure 2 shows the XRD patterns of the three samples. The characteristic peaks present within  $10\text{--}20^\circ$  our synthesized ZIF-8-coated ZnO can correspond to ZIF-8, and the diffraction peaks in the range of  $30\text{--}70^\circ$  can correspond to the standard spectrum of ZnO (JDPDS card: 36-1451). ZIF-8 and ZIF-8-coated ZnO were prepared by us, and their XRD patterns are consistent with those in the literature [45,58,59]. A closer look reflects that the diffraction peak intensity of ZIF-8 in the complex is lower than that of pure ZIF-8, we speculate for two reasons: Firstly, the content of ZIF-8 may be lower [60], and secondly, the sacrificial preparation of ZIF-8 on ZnO may have some effect on its crystallinity [55]. Furthermore, no other impurity peaks appeared on the spectrum, which proves the successful synthesis of the composite.

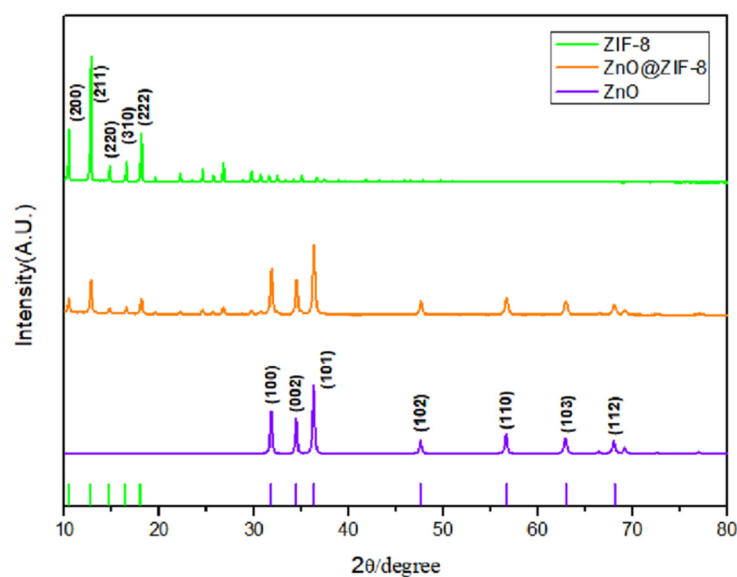


**Figure 2.** XRD patterns of ZnO nanorods, ZIF-8 and ZIF-8-coated ZnO.

### 3.1.2. SEM and TEM Analysis

SEM and TEM images were used to observe the changes in size and morphology of the materials before and after MOF synthesis. For the SEM and TEM images of the ZnO before recombination (Figure 3a,c), in the figure presented to us, the as-synthesized ZnO is in the shape of rods. The rods are clustered into clusters, and the end result resembles a sea urchin, with a very smooth surface and a diameter of about 268 nm. Whereas after sacrificing ZnO to obtain the attached ZIF-8 shell, the micromorphology of the obtained ZIF-8-attached ZnO is shown in Figure 3b,d. Obviously, SEM shows that the diameter and length of the rods increased sharply, and the surface became very rough. If you look closely, you can find that the surface attachments have a certain shape. It can be considered that the rhombic dodecahedron ZIF-8 was successfully synthesized. It is clear that the reaction product is a core-shell structure, and the ZnO does not disappear completely, but retains a part. Since the degree of etching is not the same, the diameter of the remaining ZnO rods is also large or small. In any case, the TEM images clearly demonstrate the formation of new species. Moreover, the conductive connection of this structure is realized by direct connection of rods (Figure 3c,d). During the gas-sensing test, these interconnected rods react with gas and conduct electrons to each other. These nanorods are then connected to electrodes on the sensor substrate to transmit electrical signals to the sensor for display.

### 3.1.3. EDS Element Analysis

To further demonstrate that ZIF-8 was successfully synthesized and to explore the distribution of MOFs, we performed EDS elemental scanning on the as-prepared ZIF-8-coated ZnO samples (Figure 4a–d). Observing the distribution map of four elements, Zn, O, C, and N, the distribution map of Zn, O elements shows that ZnO is mainly distributed in the central part of the composite, which corresponds to the opaque core region in the TEM image, which shows that the main distribution component of this part is ZnO. The distribution of C and N elements, which are the iconic elements of ZIF-8, represents the position of ZIF-8, which corresponds to the light-colored transparent shell-like area in the TEM image, which shows that the ZIF-8 successfully encapsulated zinc oxide.

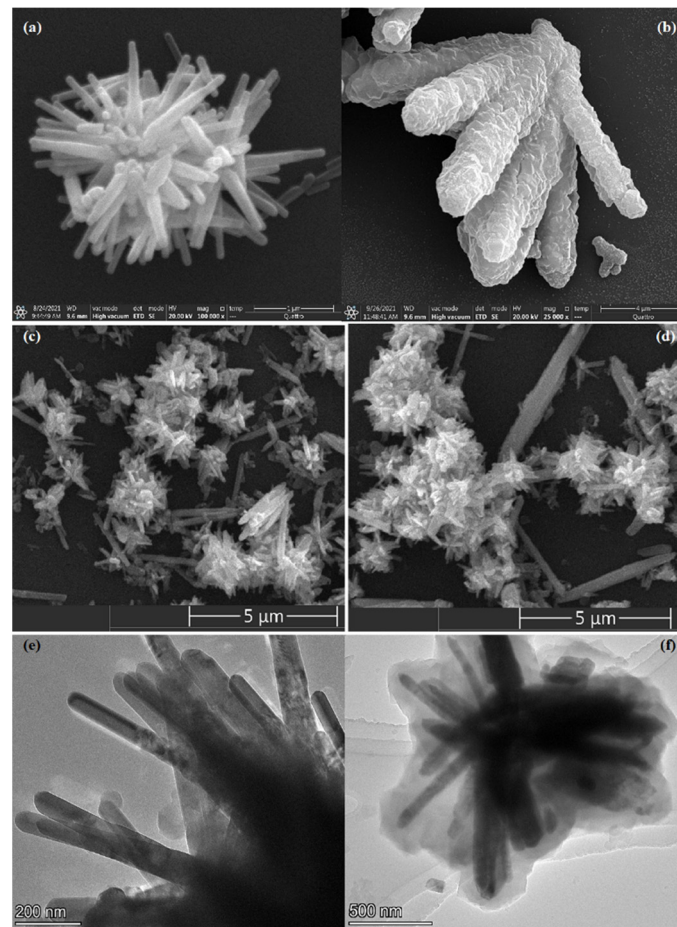


**Figure 3.** The SEM images and the TEM images of (a,c–e) ZnO nanorods, (b,f) ZIF-8-coated ZnO.

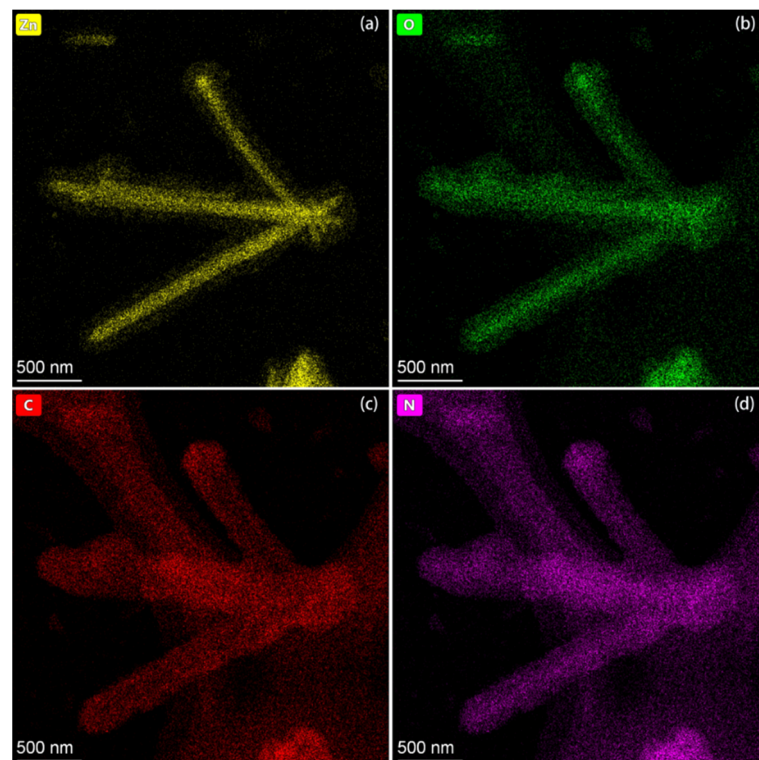


**Figure 4.** EDS elemental mappings of ZIF-8-coated ZnO: (a) Zn, (b) O, (c) C, and (d) N.

### 3.1.4. TG Analysis

Because the optimal working temperature of ZnO is known to be relatively high, in order to compare the gas-sensing properties before and after the composite, we carried out a thermogravimetric (TG) experiment on the ZIF-8-coated ZnO sample, which was mainly to observe the thermal stability of the composite material. The results of the TG experiment are shown in Figure 5. The initial weight of the sample was 6.64 mg, and when we calcined it to 400 °C, the weight loss was only 1.923%. Within the allowable error range, it shows that the structure of the composite material is not greatly damaged or collapsed at 400 °C. TG experiments show that the composites prepared by us can maintain high thermal stability at high temperatures, and the gas-sensing properties can be tested at high working temperatures. The thermal decomposition product of ZIF-8 in air is ZnO, which also avoids the possible interference of the thermal decomposition of ZIF-8 with the final experimental results.

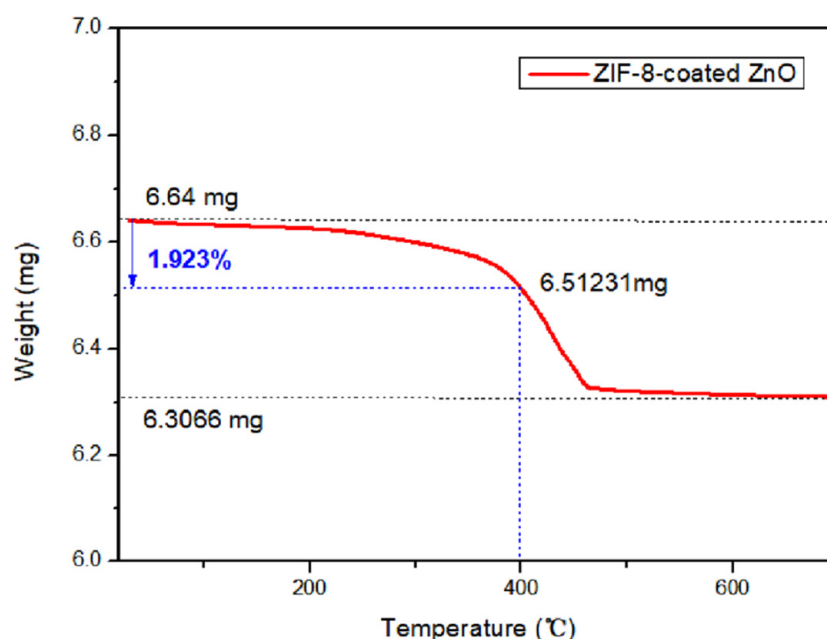
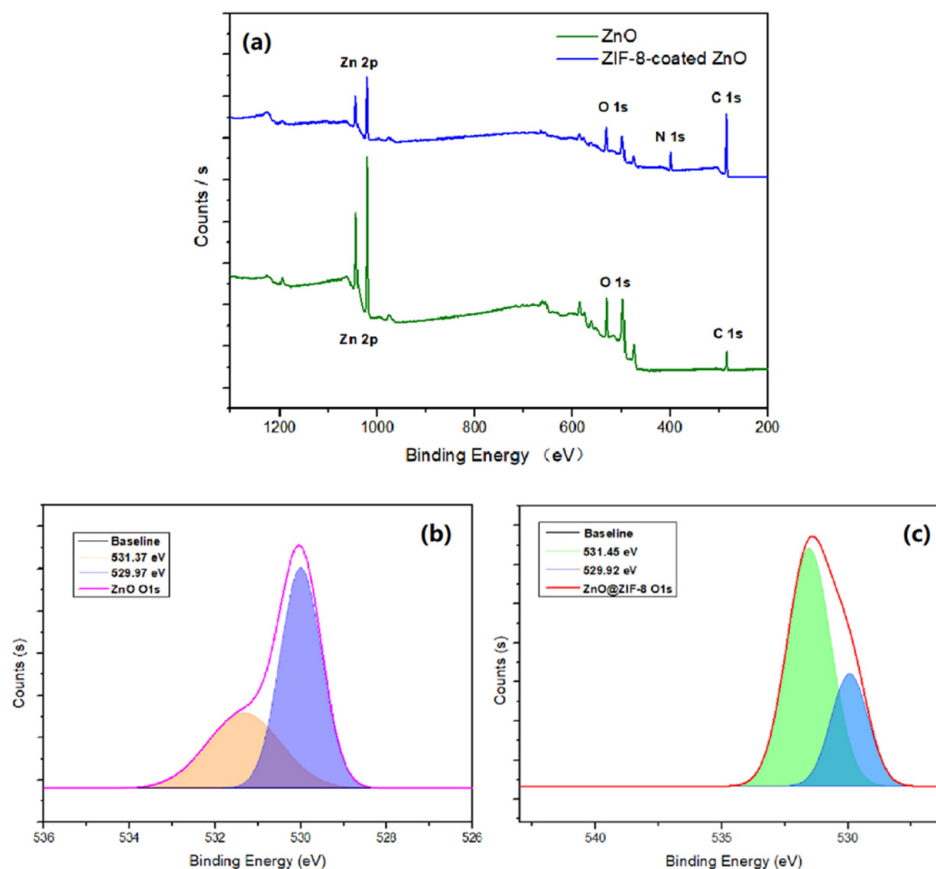


Figure 5. Thermogravimetric analysis of ZIF-8-coated ZnO.

### 3.1.5. XPS Analysis

Then we also analyzed the elements of the material, using XPS technology to analyze the element changes before and after compounding. From the whole spectrum (Figure 6a), it can be observed that N element appears after compounding, which is attributed to the fact that organic ligands in ZIF-8 contain N, while ZnO does not. In addition, the C element should be contained after compounding, but ZnO also contains a small amount of C element, which is due to the influence of the test substrate in the XPS experiment. The content of Zn decreased after recombination. As XPS mainly detects the element distribution of the surface layer of the material, it shows that ZIF-8 ( $C_8H_{10}N_4Zn$ ) is the main component in the surface layer, and the Zn content is low. In a word, through the measurement of the whole spectrum, it can also be shown that part of ZnO is converted into ZIF-8 containing C element and N element and a little Zn. Among all kinds of elements, the peak distribution of O 1s has the greatest relationship with gas-sensing performance. From the XPS peak (Figure 6b,c), it can be seen that the area of the energy peak before and after O 1s changed. Before compounding, the low-energy peak (the peak represented by lattice oxygen) of the original ZnO has a large area (529.97 eV), while the high-energy peak (531.37 eV) accounts for a small proportion. However, after compounding, the peak area of lattice oxygen decreases, the proportion decreases, and the peak area represented by oxygen defects increases significantly, which indicates that the lattice oxygen of ZnO is partially

decomposed, and the ZnO part is transformed into ZIF-8. The material can provide more adsorption and reaction sites for the reaction between ethanol with the sensor materials, and these defects are beneficial to further increasing the adsorption of oxygen. Note that there is a slight difference in the energy of the O 1s peaks before and after compounding, which is within the error range and therefore can be basically ignored.



**Figure 6.** (a) XPS full spectrum and the peaks of O 1s of (b) ZnO and (c) ZIF-8-coated ZnO.

### 3.2. The Formation of ZIF-8-Coated ZnO Structure

The specific process of the formation of ZIF-8-coated ZnO is as follows (Figure 7). The organic ligand 2-methylimidazole and the prepared ZnO powder were added to the solvent ethanol, and no reaction occurred at room temperature. Then heating at 50 °C, the ZnO surface dissolves and release zinc ions. The zinc ions coordinate and react with 2-methylimidazole in solution to generate ZIF-8 and nucleate and grow on ZnO, gradually forming a ZIF-8 shell. Since zinc ions and organic ligands can pass through the pores of ZIF-8, zinc ions continue to be released and diffuse into the solution from the interface of ZnO and ZIF-8, where ZIF-8 grows out at the interface of ZIF-8 and the solution [52,61,62]. At the same time, 2-methylimidazole diffused into the pores, came to the interface of the metal oxide and MOF, and reacted with Zn ions to generate ZIF-8 inward. Therefore, with the passage of time, the simultaneous generation of ZIF-8 in and out makes the shell layer uniform and the thickness gradually increases, and finally a material with a core-shell structure is obtained.



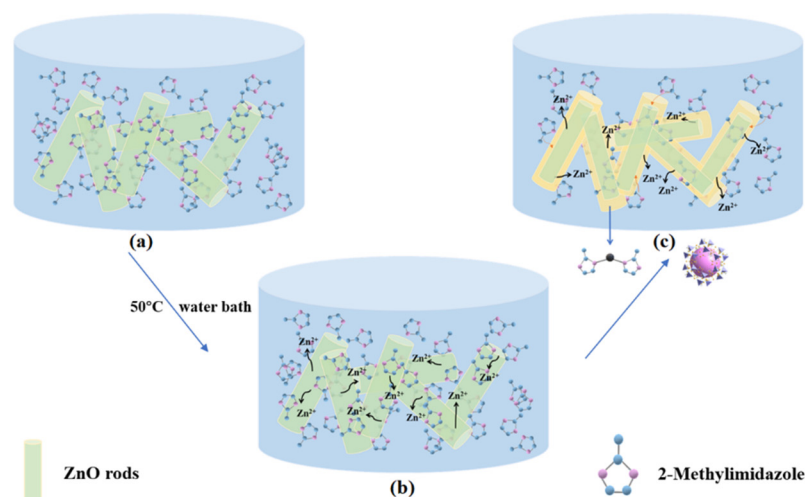


**Figure 7.** Growth process of ZIF-8. (a,b) A green rod represents a ZnO rod and the ball-and-stick model represents a 2-methylimidazole molecule. (c) The yellow shell on the surface of the green ZnO rod represents ZIF-8, whose ball-and-stick model and topology have been given in the figure.

### 3.3. Gas-Sensing Property

We conducted a series of gas-sensing tests to explore the effect of this combination on the detection performance of ZnO. Figure 8a,b are the instantaneous resistance changes of ethanol vapor with the same concentration at the same temperature. It can be seen that the resistance change of the composite material is larger and more obvious, indicating that it has a greater response to ethanol gas. In the case of temperature and concentration changes, the sensor responses of the two materials were further tested to prove that these results are universal for a wide range of temperatures and concentration. The gas responses at different temperatures in 20 ppm ethanol are shown in Figure 8c. After ZIF-8 coating, the response to ethanol was significantly improved, although the optimal operating temperature was still 350 °C. At 350 °C, the response value to ethanol vapor is more than twice that of the original value. We believe that the optimum temperature did not decrease because ZIF-8 is only used as functional material here, while ZnO is used as active material. Therefore, it is actually the ZnO that transfers electrons and reacts with ethanol before and after compounding. At 350 °C, the response of ZIF-8-coated ZnO is increased by about 110%, which is mainly because there are more defects on the surface of ZnO due to etching of ZnO before and after compounding, so the adsorption sites increased, and the response improved.

Figure 8d shows that at 350 °C, in the concentration range of 10–80 ppm, the responses of the two samples increased with increasing ethanol concentration. The response increase in ZIF-8-coated ZnO is more significant and the response is always higher than that of raw ZnO. When the concentration was 80 ppm, the response of the sensor increases from 25.0 to 56.7. This shows that the increase in defects at the interface increases the amount of adsorbed oxygen, thus the number of transferred electrons increases, and the change of resistance becomes larger. Furthermore, Figure 8e,f shows the response and recovery time curves for 20 ppm ethanol. The response recovery time of pure ZnO is 5 s and 4 s, respectively, and the time after compounding is 8 s and 5 s, respectively. Although the speed is slightly slower, it is very fast. Some previous reports found that the response recovery rate was much slower after the production of ZIF-8 because the pore size limited the diffusion rate of gas molecules [59,63]. The response recovery characteristics of the composite material obtained in this work are very good. We speculate that on the one hand, because the thickness of ZIF-8 is not too thick, the gas diffusion path is not too long. Regarding the control of the thickness of ZIF-8, it mainly depends on the reaction time [52,53]. If the composite reaction time is shortened, ZIF-8 may not be able to completely encapsulate ZnO, and too long a reaction time also leads to the thickening of the shell layer of ZIF-8. This has also been explored in some previous reports [45,64]. In conclusion,

it is also important to control a reasonable ZIF-8 shell thickness. On the other hand, the pore size is larger than the theoretical size, so the hindering ability of gas molecules is also reduced.

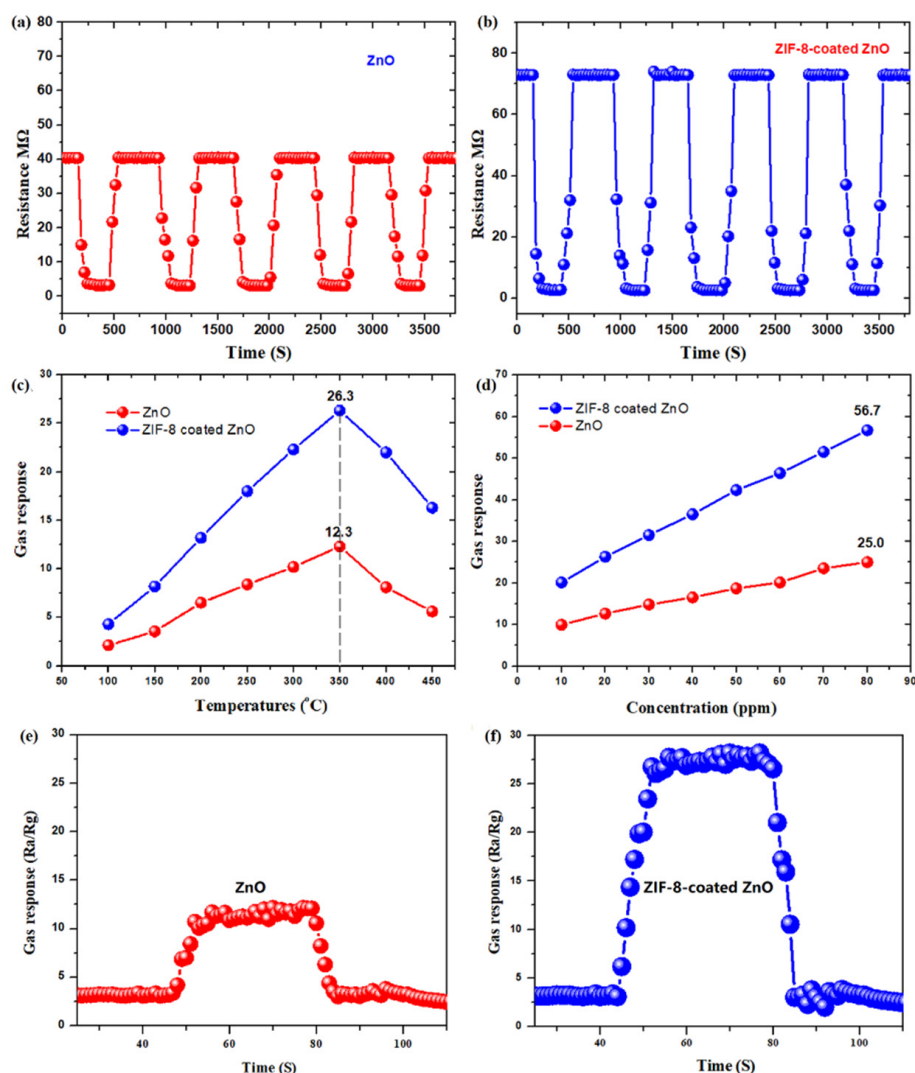


**Figure 8.** (a,b) Instantaneous resistance change of two materials. Response of two samples (c) towards 20 ppm ethanol at different temperatures, (d) in different concentrations of ethanol at 350 °C. (e,f) Response-recovery characteristics of two samples to 20 ppm ethanol at 350 °C.

### 3.4. Gas-Sensing Mechanism

As shown in Figure 9, due to the use of ZnO as the active material, it can be directly explained by the gas-sensing mechanism of the raw material ZnO [65,66]. In air, oxygen adsorbs on ZnO and accepts electrons to become oxygen species, ZnO generates the electron depletion layer, and the resistance increases. In reducing ethanol, the ethanol donates electrons for the redox reaction, and the resistance of ZnO decreases [67]. As a functional material, ZIF-8 mainly increases the adsorption of oxygen by increasing the specific surface area, while the interface of ZnO and MOF generates defects, thereby increasing the active sites. The improvement of gas sensitivity can also be put down to the increase in oxygen vacancies, which can provide more active sites for the adsorption of target gas molecules [68]. The change of oxygen vacancies can be explained by the change of the O 1s peak area ratio of XPS before and after compounding. The lower energy peaks represent lattice oxygen, and it can be seen that the content of lattice oxygen decreases before and after the reaction, which indicates that the content of ZnO containing lattice oxygen decreases and ZnO is converted to other products [69,70]. The higher energy peaks

represent oxygen defects, and the increase in the content of oxygen defects explains the increased response [59,71,72]. In addition, the pores of ZIF-8 can also act as a layer of sieving to prevent the entry of macromolecules. Since the prepared ZIF-8 framework is flexible, it allows the entry of ethanol molecules and allows the reaction products to be released smoothly. Due to the above points, the gas-sensing performance is improved.

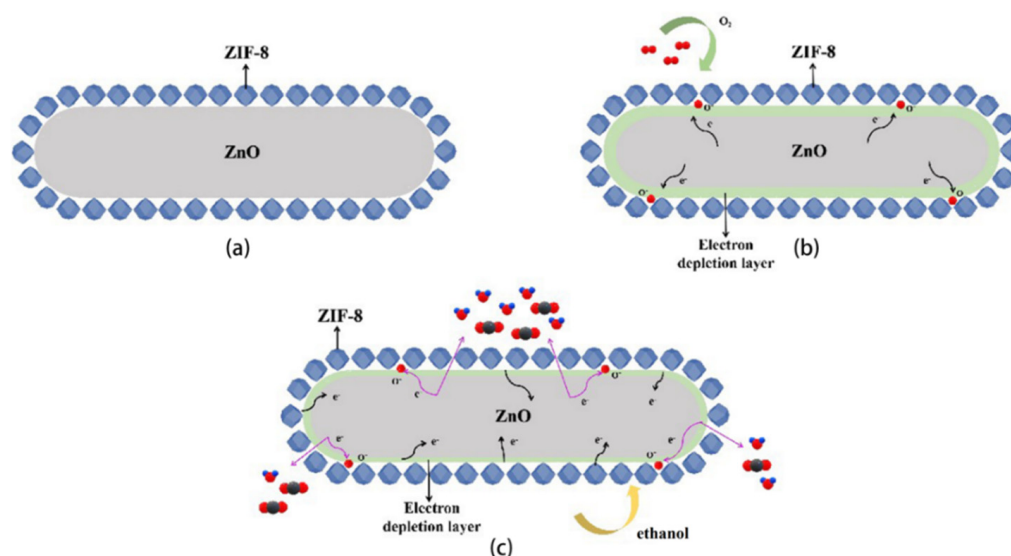


**Figure 9.** Gas-sensing mechanism of ZIF-8-coated ZnO (a) in air and (b) in ethanol. (c) The black balls represent carbon atoms, the blue balls represent hydrogen atoms, and the red balls represent oxygen atoms.

The diameter of ethanol molecules (4.53 Å) is actually larger than that (3.4 Å) of the ZIF-8. However, many previous reports have also established that ethanol molecules can enter ZIF-8 and be detected by ZnO@ZIF-8 [68,73]. These reports suggest that the entry of ethanol molecules due to the structure of ZIF-8 is flexible [41]. Therefore, it can adsorb molecules slightly larger than its pore size, but theoretically, even if the functional group can oscillate, the maximum access diameter is around 4 Å, the entry of ethanol molecules indicates that it is not only the reason for the structural flexibility of ZIF-8 [74]. We performed a measurement on the pore size of the synthesized ZnO@ZIF-8 material and the raw ZnO. As shown in Figure 10, the pore size of our synthesized composites is concentrated around 3.9 Å, which is slightly larger than the theoretical value, which indicates that in addition to the flexibility of the framework itself, it may also be due to the Zn ions produced by ZnO-produced structural defects during the reaction, which expanded the pore of ZIF-8 obtained by sacrificial transformation [12,75]. The surface of ZnO is smooth, with few pores and small pore volume. This experimental result also provides a possible method for the detection of gas molecules that are slightly larger than that of ZIF-8.

In addition, compared with some previous experimental methods, this experiment also reduced the experimental temperature, which makes the preparation more energy-efficient, which is also an advantage of this method.

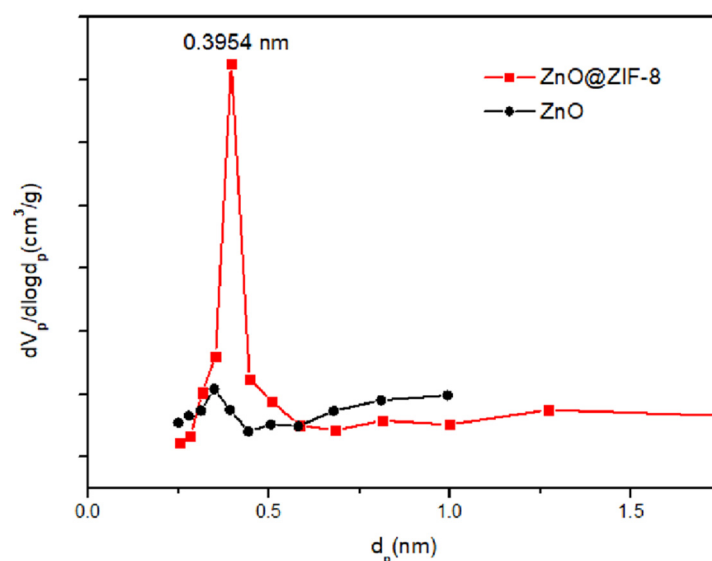


Figure 10. Pore size distribution of raw ZnO and composite products.

#### 4. Conclusions

In this work, we fabricated rod-shaped ZnO as well as ZIF-8-coated ZnO and performed some performance tests. The response to ethanol gas was enhanced due to the porosity of ZIF-8. Although there are many strategies to improve the gas-sensing properties of ZnO, the synthetic method we used and the prepared product are promising, mainly because of its simple preparation method, low cost, and energy saving. ZnO itself provides metal ions for ZIF-8 as a Zn<sup>2+</sup> source, and the adhesion amount of ZIF-8 can be easily adjusted by changing the experimental conditions (such as the amount of 2-methylimidazole, reaction time, and solvent). The simple preparation of porous structures and the improvement of sensing performance obtained in this experiment provide some ideas for the synthesis and future applications of functional metal oxides.

**Author Contributions:** Conceptualization, B.H.; methodology, B.H.; software, W.Z.; validation, W.Z.; formal analysis, B.H.; investigation, B.H.; resources, W.Z.; data curation, B.H.; writing—original draft preparation, B.H.; writing—review and editing, W.Z.; visualization, Y.L.; supervision, Y.L.; project administration, Y.L.; funding acquisition, Y.L. All authors have read and agreed to the published version of the manuscript.

**Funding:** This work was supported by Technological innovation and application development of Chongqing Talent Project (Grant No. cstc2021ycjh-bgzxm0341) and the Science and Technology Research Program of Chongqing Municipal Education Commission (No. KJQN201801320).

**Institutional Review Board Statement:** Not applicable.

**Informed Consent Statement:** Informed consent was obtained from all subjects involved in the study.

**Data Availability Statement:** The data is available on the request from corresponding author.

**Conflicts of Interest:** The authors declare no conflict of interest.

#### References

- Lu, J.; Li, B.; Li, H.; Al-Barakani, A. Expansion of city scale, traffic modes, traffic congestion, and air pollution. *Cities* **2021**, *108*, 102974. [CrossRef]
- Shaddick, G.; Thomas, M.L.; Mudu, P.; Ruggeri, G.; Gummy, S. Half the world's population are exposed to increasing air pollution. *Npj Clim. Atmos. Sci.* **2020**, *3*, 23. [CrossRef]
- Molev, M.; Zanina, I.; Chertov, Y.; Shemetov, A. Assessment of urban environment safety for public health. In Proceedings of the International Scientific Conference on Business Technologies for Sustainable Urban Development (SPbWOSCE), Peter Great Saint Petersburg Polytechnic University, Institute Ind Management Econ & Tr, St Petersburg, Russia, 20–22 December 2017.

4. Lajunen, A.; Lipman, T. Lifecycle cost assessment and carbon dioxide emissions of diesel, natural gas, hybrid electric, fuel cell hybrid and electric transit buses. *Energy* **2016**, *106*, 329–342. [[CrossRef](#)]
5. Jiang, W.; Lu, C.; Miao, Y.; Xiang, Y.; Chen, L.; Deng, Q. Outdoor particulate air pollution and indoor renovation associated with childhood pneumonia in China. *Atmos. Environ.* **2018**, *174*, 76–81. [[CrossRef](#)]
6. Palacios, J.; Eichholtz, P.; Kok, N.; Aydin, E. The impact of housing conditions on health outcomes. *Real Estate Econ.* **2021**, *49*, 1172–1200. [[CrossRef](#)]
7. Ren, P.; Qi, L.; You, K.; Shi, Q. Hydrothermal Synthesis of Hierarchical SnO<sub>2</sub> Nanostructures for Improved Formaldehyde Gas Sensing. *Nanomaterials* **2022**, *12*, 228. [[CrossRef](#)]
8. Dadkhah, M.; Tulliani, J.-M. Nanostructured Metal Oxide Semiconductors towards Greenhouse Gas Detection. *Chemosensors* **2022**, *10*, 57. [[CrossRef](#)]
9. Nasriddinov, A.; Tokarev, S.; Fedorova, O.; Bozhev, I.; Rummyantseva, M. In<sub>2</sub>O<sub>3</sub> Based Hybrid Materials: Interplay between Microstructure, Photoelectrical and Light Activated NO<sub>2</sub> Sensor Properties. *Chemosensors* **2022**, *10*, 135. [[CrossRef](#)]
10. Chizhov, A.; Kutukov, P.; Gulina, A.; Astafiev, A.; Rummyantseva, M. UV-Activated NO<sub>2</sub> Gas Sensing by Nanocrystalline ZnO: Mechanistic Insights from Mass Spectrometry Investigations. *Chemosensors* **2022**, *10*, 147. [[CrossRef](#)]
11. Xue, S.; Cao, S.; Huang, Z.; Yang, D.; Zhang, G. Improving Gas-Sensing Performance Based on MOS Nanomaterials: A Review. *Materials* **2021**, *14*, 4263. [[CrossRef](#)]
12. Liu, Q.; Low, Z.-X.; Li, L.; Razmjou, A.; Wang, K.; Yao, J.; Wang, H. ZIF-8/Zn<sub>2</sub>GeO<sub>4</sub> nanorods with an enhanced CO<sub>2</sub> adsorption property in an aqueous medium for photocatalytic synthesis of liquid fuel. *J. Mater. Chem. A* **2013**, *1*, 11563–11569. [[CrossRef](#)]
13. Peng, P.; Deng, Y.; Niu, J.; Shi, L.; Mei, Y.; Du, S.; Liu, J.; Xu, D. Fabrication and electrical characteristics of flash-sintered SiO<sub>2</sub>-doped ZnO-Bi<sub>2</sub>O<sub>3</sub>-MnO(2) varistors. *J. Adv. Ceram.* **2020**, *9*, 683–692. [[CrossRef](#)]
14. Kumar, R.R.; Murugesan, T.; Chang, T.-W.; Lin, H.-N. Defect controlled adsorption/desorption kinetics of ZnO nanorods for UV-activated NO<sub>2</sub> gas sensing at room temperature. *Mater. Lett.* **2021**, *287*, 129257. [[CrossRef](#)]
15. Zhu, L.; Zeng, W. Room-temperature gas sensing of ZnO-based gas sensor: A review. *Sens. Actuators A Phys.* **2017**, *267*, 242–261. [[CrossRef](#)]
16. Zheng, K.-G.; Yang, T.-Y.; Guo, Z. Porous Pb-Doped ZnO Nanobelts with Enriched Oxygen Vacancies: Preparation and Their Chemiresistive Sensing Performance. *Chemosensors* **2022**, *10*, 96. [[CrossRef](#)]
17. Leonardi, S.G. Two-Dimensional Zinc Oxide Nanostructures for Gas Sensor Applications. *Chemosensors* **2017**, *5*, 17. [[CrossRef](#)]
18. Hui, G.; Zhu, M.; Yang, X.; Liu, J.; Pan, G.; Wang, Z. Highly sensitive ethanol gas sensor based on CeO<sub>2</sub>/ZnO binary heterojunction composite. *Mater. Lett.* **2020**, *278*, 128453. [[CrossRef](#)]
19. Xu, X.H.; Ma, S.Y.; Xu, X.L.; Han, T.; Pei, S.T.; Tie, Y.; Cao, P.F.; Liu, W.W.; Wang, B.J.; Zhang, R.; et al. Ultra-sensitive glycol sensing performance with rapid-recovery based on heterostructured ZnO-SnO<sub>2</sub> hollow nanotube. *Mater. Lett.* **2020**, *273*, 127967. [[CrossRef](#)]
20. Badadhe, S.S.; Mulla, I.S. Effect of aluminium doping on structural and gas sensing properties of zinc oxide thin films deposited by spray pyrolysis. *Sens. Actuators B Chem.* **2011**, *156*, 943–948. [[CrossRef](#)]
21. Fan, C.; Sun, F.; Wang, X.; Majidi, M.; Huang, Z.; Kumar, P.; Liu, B. Enhanced H<sub>2</sub>S gas sensing properties by the optimization of p-CuO/n-ZnO composite nanofibers. *J. Mater. Sci.* **2020**, *55*, 7702–7714. [[CrossRef](#)]
22. Al-Hadeethi, Y.; Umar, A.; Ibrahim, A.A.; Al-Heniti, S.H.; Kumar, R.; Baskoutas, S.; Raffah, B.M. Synthesis, characterization and acetone gas sensing applications of Ag-doped ZnO nanoneedles. *Ceram. Int.* **2017**, *43*, 6765–6770. [[CrossRef](#)]
23. Huang, J.; Zhou, J.; Liu, Z.; Li, X.; Geng, Y.; Tian, X.; Du, Y.; Qian, Z. Enhanced acetone-sensing properties to ppb detection level using Au/Pd-doped ZnO nanorod. *Sens. Actuators B Chem.* **2020**, *310*, 127129. [[CrossRef](#)]
24. Krishna, K.G.; Parne, S.; Pothukanuri, N.; Kathirvelu, V.; Gandhi, S.; Joshi, D. Nanostructured metal oxide semiconductor-based gas sensors: A comprehensive review. *Sens. Actuators A Phys.* **2022**, *341*, 113578. [[CrossRef](#)]
25. Kang, Y.; Yu, F.; Zhang, L.; Wang, W.; Chen, L.; Li, Y. Review of ZnO-based nanomaterials in gas sensors. *Solid State Ion.* **2021**, *360*, 115544. [[CrossRef](#)]
26. Chen, H.; Liu, Y.; Xie, C.; Wu, J.; Zeng, D.; Liao, Y. A comparative study on UV light activated porous TiO<sub>2</sub> and ZnO film sensors for gas sensing at room temperature. *Ceram. Int.* **2012**, *38*, 503–509. [[CrossRef](#)]
27. Gogurla, N.; Sinha, A.K.; Santra, S.; Manna, S.; Ray, S.K. Multifunctional Au-ZnO Plasmonic Nanostructures for Enhanced UV Photodetector and Room Temperature NO Sensing Devices. *Sci. Rep.* **2014**, *4*, 6483. [[CrossRef](#)]
28. Zhang, J.; Liu, X.; Neri, G.; Pinna, N. Nanostructured Materials for Room-Temperature Gas Sensors. *Adv. Mater.* **2016**, *28*, 795–831. [[CrossRef](#)]
29. Nakate, U.T.; Patil, P.; Bulakhe, R.N.; Lokhande, C.D.; Kale, S.N.; Naushad, M.; Mane, R.S. Sprayed zinc oxide films: Ultra-violet light-induced reversible surface wettability and platinum-sensitization-assisted improved liquefied petroleum gas response. *J. Colloid Interface Sci.* **2016**, *480*, 109–117. [[CrossRef](#)]
30. Franke, M.E.; Koplín, T.J.; Simon, U. Metal and metal oxide nanoparticles in chemiresistors: Does the nanoscale matter? *Small* **2006**, *2*, 36–50. [[CrossRef](#)]
31. Bhat, P.; Kumar, N.S.K.; Nagaraju, P. Synthesis and characterization of ZnO-MWCNT nanocomposites for 1-butanol sensing application at room temperature. *Phys. B Condens. Matter* **2019**, *570*, 139–147. [[CrossRef](#)]
32. Li, Y.; Jiao, M.; Yang, M. In-situ grown nanostructured ZnO via a green approach and gas sensing properties of polypyrrole/ZnO nanohybrids. *Sens. Actuators B Chem.* **2017**, *238*, 596–604. [[CrossRef](#)]

33. Han, C.; Li, X.; Shao, C.; Li, X.; Ma, J.; Zhang, X.; Liu, Y. Composition-controllable p-CuO/n-ZnO hollow nanofibers for high-performance H<sub>2</sub>S detection. *Sens. Actuators B Chem.* **2019**, *285*, 495–503. [[CrossRef](#)]
34. Huang, B.; Li, Y.; Zeng, W. Application of Metal-Organic Framework-Based Composites for Gas Sensing and Effects of Synthesis Strategies on Gas-Sensitive Performance. *Chemosensors* **2021**, *9*, 226. [[CrossRef](#)]
35. Talin, A.A.; Centrone, A.; Ford, A.C.; Foster, M.E.; Stavila, V.; Haney, P.; Kinney, R.A.; Szalai, V.; El Gabaly, F.; Yoon, H.P.; et al. Tunable Electrical Conductivity in Metal-Organic Framework Thin-Film Devices. *Science* **2014**, *343*, 66–69. [[CrossRef](#)]
36. Campbell, M.G.; Dinca, M. Metal-Organic Frameworks as Active Materials in Electronic Sensor Devices. *Sensors* **2017**, *17*, 1108. [[CrossRef](#)]
37. Yi, F.-Y.; Chen, D.; Wu, M.-K.; Han, L.; Jiang, H.-L. Chemical Sensors Based on Metal-Organic Frameworks. *Chempluschem* **2016**, *81*, 675–690. [[CrossRef](#)] [[PubMed](#)]
38. Li, H.-Y.; Zhao, S.-N.; Zang, S.-Q.; Li, J. Functional metal-organic frameworks as effective sensors of gases and volatile compounds. *Chem. Soc. Rev.* **2020**, *49*, 6364–6401. [[CrossRef](#)]
39. Kukkar, P.; Kim, K.-H.; Kukkar, D.; Singh, P. Recent advances in the synthesis techniques for zeolitic imidazolate frameworks and their sensing applications. *Coord. Chem. Rev.* **2021**, *446*, 214109. [[CrossRef](#)]
40. Duan, C.X.; Yu, Y.; Hu, H. Recent progress on synthesis of ZIF-67-based materials and their application to heterogeneous catalysis. *Green Energy Environ.* **2022**, *7*, 3–15. [[CrossRef](#)]
41. Phan, A.; Doonan, C.J.; Uribe-Romo, F.J.; Knobler, C.B.; O’Keeffe, M.; Yaghi, O.M. Synthesis, Structure, and Carbon Dioxide Capture Properties of Zeolitic Imidazolate Frameworks. *Acc. Chem. Res.* **2010**, *43*, 58–67. [[CrossRef](#)]
42. Sun, J.; Sun, L.; Bai, S.; Fu, H.; Guo, J.; Feng, Y.; Luo, R.; Li, D.; Chen, A. Pyrolyzing Co/Zn bimetallic organic framework to form p-n heterojunction of Co<sub>3</sub>O<sub>4</sub>/ZnO for detection of formaldehyde. *Sens. Actuators B Chem.* **2019**, *285*, 291–301. [[CrossRef](#)]
43. Yao, M.-S.; Li, W.-H.; Xu, G. Metal-organic frameworks and their derivatives for electrically-transduced gas sensors. *Coord. Chem. Rev.* **2021**, *426*, 213479. [[CrossRef](#)]
44. Huang, B.; Zeng, W.; Li, Y. Synthesis of ZnO@ZIF-8 Nanorods with Enhanced Response to VOCs. *J. Electrochem. Soc.* **2022**, *169*, 047508. [[CrossRef](#)]
45. Tian, H.; Fan, H.; Li, M.; Ma, L. Zeolitic Imidazolate Framework Coated ZnO Nanorods as Molecular Sieving to Improve Selectivity of Formaldehyde Gas Sensor. *ACS Sens.* **2016**, *1*, 243–250. [[CrossRef](#)]
46. Zhan, K.; Xing, Y.; Zhu, Y.; Yan, J.; Chen, Y. Carbon tetrachloride vapor sensing based on ZIF-8@ZnO/TiO<sub>2</sub> one-dimensional top-defect photonic crystals. *Sens. Actuators A Phys.* **2020**, *314*, 112249. [[CrossRef](#)]
47. Park, K.S.; Ni, Z.; Cote, A.P.; Choi, J.Y.; Huang, R.; Uribe-Romo, F.J.; Chae, H.K.; O’Keeffe, M.; Yaghi, O.M. Exceptional chemical and thermal stability of zeolitic imidazolate frameworks. *Proc. Natl. Acad. Sci. USA* **2006**, *103*, 10186–10191. [[CrossRef](#)]
48. Matatagui, D.; Sainz-Vidal, A.; Gracia, I.; Figueras, E.; Cane, C.; Saniger, J.M. Chemoresistive gas sensor based on ZIF-8/ZIF-67 nanocrystals. *Sens. Actuators B Chem.* **2018**, *274*, 601–608. [[CrossRef](#)]
49. Du, B.; Cai, M.; Wang, X.; Qian, J.; He, C.; Shui, A. Enhanced electromagnetic wave absorption property of binary ZnO/NiCo<sub>2</sub>O<sub>4</sub> composites. *J. Adv. Ceram.* **2021**, *10*, 832–842. [[CrossRef](#)]
50. Drobek, M.; Kim, J.-H.; Bechelany, M.; Vallicari, C.; Julbe, A.; Kim, S.S. MOF-Based Membrane Encapsulated ZnO Nanowires for Enhanced Gas Sensor Selectivity. *ACS Appl. Mater. Interfaces* **2016**, *8*, 8323–8328. [[CrossRef](#)]
51. Zhou, T.; Sang, Y.; Sun, Y.; Wu, C.; Wang, X.; Tang, X.; Zhang, T.; Wang, H.; Xie, C.; Zeng, D. Gas Adsorption at Metal Sites for Enhancing Gas Sensing Performance of ZnO@ZIF-71 Nanorod Arrays. *Langmuir* **2019**, *35*, 3248–3255. [[CrossRef](#)]
52. Wu, X.; Xiong, S.; Mao, Z.; Hu, S.; Long, X. A Designed ZnO@ZIF-8 Core-Shell Nanorod Film as a Gas Sensor with Excellent Selectivity for H<sub>2</sub> over CO. *Chem. A Eur. J.* **2017**, *23*, 7969–7975. [[CrossRef](#)]
53. Lv, R.; Zhang, Q.; Wang, W.; Lin, Y.; Zhang, S. ZnO@ZIF-8 Core-Shell Structure Gas Sensors with Excellent Selectivity to H<sub>2</sub>. *Sensors* **2021**, *21*, 4069. [[CrossRef](#)]
54. Yao, M.-S.; Tang, W.-X.; Wang, G.-E.; Nath, B.; Xu, G. MOF Thin Film-Coated Metal Oxide Nanowire Array: Significantly Improved Chemiresistor Sensor Performance. *Adv. Mater.* **2016**, *28*, 5229–5244. [[CrossRef](#)] [[PubMed](#)]
55. Liu, Y.; Wang, R.; Zhang, T.; Liu, S.; Fei, T. Zeolitic imidazolate framework-8 (ZIF-8)-coated In<sub>2</sub>O<sub>3</sub> nanofibers as an efficient sensing material for ppb-level NO<sub>2</sub> detection. *J. Colloid Interface Sci.* **2019**, *541*, 249–257. [[CrossRef](#)] [[PubMed](#)]
56. Zhou, Y.; Zhou, T.; Zhang, Y.; Tang, L.; Guo, Q.; Wang, M.; Xie, C.; Zeng, D. Synthesis of core-shell flower-like WO<sub>3</sub>@ZIF-71 with enhanced response and selectivity to H<sub>2</sub>S gas. *Solid State Ion.* **2020**, *350*, 115278. [[CrossRef](#)]
57. Dmello, M.E.; Sundaram, N.G.; Kalidindi, S.B. Assembly of ZIF-67 Metal-Organic Framework over Tin Oxide Nanoparticles for Synergistic Chemiresistive CO<sub>2</sub> Gas Sensing. *Chem. A Eur. J.* **2018**, *24*, 9220–9223. [[CrossRef](#)]
58. Zhou, T.; Sang, Y.; Wang, X.; Wu, C.; Zeng, D.; Xie, C. Pore size dependent gas-sensing selectivity based on ZnO@ZIF nanorod arrays. *Sens. Actuators B Chem.* **2018**, *258*, 1099–1106. [[CrossRef](#)]
59. Cui, F.; Chen, W.; Jin, L.; Zhang, H.; Jiang, Z.; Song, Z. Fabrication of ZIF-8 encapsulated ZnO microrods with enhanced sensing properties for H<sub>2</sub> detection. *J. Mater. Sci. Mater. Electron.* **2018**, *29*, 19697–19709. [[CrossRef](#)]
60. Ji, P.; Hu, X.; Tian, R.; Zheng, H.; Sun, J.; Zhang, W.; Peng, J. Atom-economical synthesis of ZnO@ZIF-8 core-shell heterostructure by dry gel conversion (DGC) method for enhanced H<sub>2</sub> sensing selectivity. *J. Mater. Chem. C* **2020**, *8*, 2927–2936. [[CrossRef](#)]
61. Nair, S.S.; Illyaskutty, N.; Tam, B.; Yazaydin, A.O.; Emmerich, K.; Steudel, A.; Hashem, T.; Schoettner, L.; Woell, C.; Kohler, H.; et al. ZnO@ZIF-8: Gas sensitive core-shell hetero-structures show reduced cross-sensitivity to humidity. *Sens. Actuators B Chem.* **2020**, *304*, 127184. [[CrossRef](#)]

62. Zhan, W.-W.; Kuang, Q.; Zhou, J.-Z.; Kong, X.-J.; Xie, Z.-X.; Zheng, L.-S. Semiconductor@Metal-Organic Framework Core-Shell Heterostructures: A Case of ZnO@ZIF-8 Nanorods with Selective Photoelectrochemical Response. *J. Am. Chem. Soc.* **2013**, *135*, 1926–1933. [[CrossRef](#)] [[PubMed](#)]
63. Khudiar, A.I.; Elttayef, A.K.; Khalaf, M.K.; Oufi, A.M. Fabrication of ZnO@ZIF-8 gas sensors for selective gas detection. *Mater. Res. Express* **2019**, *6*, 126450. [[CrossRef](#)]
64. Yao, M.-S.; Cao, L.-A.; Tang, Y.-X.; Wang, G.-E.; Liu, R.-H.; Kumar, P.N.; Wu, G.-D.; Deng, W.-H.; Hong, W.-J.; Xu, G. Gas transport regulation in a MO/MOF interface for enhanced selective gas detection. *J. Mater. Chem. A* **2019**, *7*, 18397–18403. [[CrossRef](#)]
65. Park, S. High-response and selective hydrogen sensing properties of porous ZnO nanotubes. *Curr. Appl. Phys.* **2016**, *16*, 1263–1269. [[CrossRef](#)]
66. Lian, X.-x.; Li, Y.; Lv, T.; Zou, Y.-l.; An, D.; Zhang, N. Preparation of ZnO Nanoparticles by Combustion Method and Their Gas Sensing Properties. *Electron. Mater. Lett.* **2016**, *12*, 24–31. [[CrossRef](#)]
67. Song, L.; Yue, H.; Li, H.; Liu, L.; Li, Y.; Du, L.; Duan, H.; Klyui, N.I. Hierarchical porous ZnO microflowers with ultra-high ethanol gas-sensing at low concentration. *Chem. Phys. Lett.* **2018**, *699*, 1–7. [[CrossRef](#)]
68. Feng, S.; Jia, X.; Yang, J.; Li, Y.; Wang, S.; Song, H. One-pot synthesis of core-shell ZIF-8@ZnO porous nanospheres with improved ethanol gas sensing. *J. Mater. Sci. Mater. Electron.* **2020**, *31*, 22534–22545. [[CrossRef](#)]
69. Kumar, V.; Swart, H.C.; Ntwaeaborwa, O.M.; Kroon, R.E.; Terblans, J.J.; Shaat, S.K.K.; Yousif, A.; Duvenhage, M.M. Origin of the red emission in zinc oxide nanophosphors. *Mater. Lett.* **2013**, *101*, 57–60. [[CrossRef](#)]
70. Islam, M.N.; Ghosh, T.B.; Chopra, K.L.; Acharya, H.N. XPS and X-ray diffraction studies of aluminum-doped zinc oxide transparent conducting films. *Thin Solid Film.* **1996**, *280*, 20–25. [[CrossRef](#)]
71. Wei, X.Q.; Man, B.Y.; Liu, M.; Xue, C.S.; Zhuang, H.Z.; Yang, C. Blue luminescent centers and microstructural evaluation by XPS and Raman in ZnO thin films annealed in vacuum, N-2 and O-2. *Phys. B Condens. Matter* **2007**, *388*, 145–152. [[CrossRef](#)]
72. Wang, J.; Wang, Z.; Huang, B.; Ma, Y.; Liu, Y.; Qin, X.; Zhang, X.; Dai, Y. Oxygen Vacancy Induced Band-Gap Narrowing and Enhanced Visible Light Photocatalytic Activity of ZnO. *Acs Appl. Mater. Interfaces* **2012**, *4*, 4024–4030. [[CrossRef](#)] [[PubMed](#)]
73. Ren, G.; Li, Z.; Yang, W.; Faheem, M.; Xing, J.; Zou, X.; Pan, Q.; Zhu, G.; Du, Y. ZnO@ZIF-8 core-shell microspheres for improved ethanol gas sensing. *Sens. Actuators B Chem.* **2019**, *284*, 421–427. [[CrossRef](#)]
74. Jafari, N.; Zeinali, S.; Shadmehr, J. Room temperature resistive gas sensor based on ZIF-8/MWCNT/AgNPs nanocomposite for VOCs detection. *J. Mater. Sci. Mater. Electron.* **2019**, *30*, 12339–12350. [[CrossRef](#)]
75. Japip, S.; Liao, K.-S.; Xiao, Y.; Chung, T.-S. Enhancement of molecular-sieving properties by constructing surface nano-metric layer via vapor cross-linking. *J. Membr. Sci.* **2016**, *497*, 248–258. [[CrossRef](#)]